

Off-design thermodynamic performances of a solar tower aided coal-fired power plant for different solar multiples with thermal energy storage

Chao Li^{a,b}, Zhiping Yang^a, Rongrong Zhai^{a,*}, Yongping Yang^a, Kumar Patchigolla^{b,*}, John E.

Oakey^b

^aSchool of Energy, Power and Mechanical Engineering, North China Electric Power University,

Beijing 102206, China

^bSchool of Water, Energy and Environment, Cranfield University, Bedford, Bedfordshire MK43

0AL, UK

*Corresponding authors: Rongrong Zhai, Kumar Patchigolla

E-mail:zhairongrong01@163.com, k.patchigolla@cranfield.ac.uk

Tel.:+86-10-61772284; +44-1234-754124; Fax: +86-10-61772284

Abstract: Solar aided coal-fired power system has been proven to be a promising way to utilise solar energy in large scale. In this paper, the performances of the solar tower aided coal-fired power (STACP) system at 100% load, 75% load, and 50% load for different days are investigated and the maximum solar power that the boiler can absorb under different plant loads are explored. Then, the effects of solar multiple (SM) and the thermal energy storage (TES) hour on the daily performance of STACP system are investigated. Results show that the maximum solar power that a 600 MW_e boiler can absorb at 100% load, 75% load and 50% load are 76.4 MW_{th}, 54.2 MW_{th} and 23.0 MW_{th}, respectively. Due to the augmented energy from the solar field, the maximum standard coal consumption rate is reduced by 13.53 g/kWh, 12.81 g/kWh and 8.22 g/kWh at 100% load, 75% load and 50% load, respectively. With an increase of solar power input, the boiler efficiency, overall system efficiency and solar thermal-to-electricity efficiency shown a downward trend. In addition,

the daily coal consumption of summer solstice is the lowest while the winter solstice is the highest for a particular SM and TES hour.

Keywords: solar energy, coal-fired power plant, solar multiple, thermal energy storage hour, renewable energy

Nomenclature

Abbreviations

CSP	Concentrated solar power
ECO	Economizer
FPS	First platen super-heater
FS	Final super-heater
HP	High pressure turbine
HR	High temperature re-heater
IP	Intermediate pressure turbine
LP	Low pressure turbine
LR	Low-temperature re-heater
MSHE	Molten salt heat exchanger
SACP	Solar aided coal-fired power system
SEP	Steam separator
SM	Solar multiple
SPS	Second platen super-heater
STACP	Solar tower aided coal-fired power system
TES	Thermal energy storage

Greek Symbols

α	solar absorptance
γ_i	specific enthalpy drop of drain water in the i_{th} heater, kJ/kg
ΔT_{exg}	temperature difference between the assumed and calculated temperature of the exit flue gas, K
$\Delta t_{FPS,in}$	temperature difference between the assumed and calculated inlet temperature of FPS, $^{\circ}C$
ΔT_{hotair}	temperature difference between the assumed and calculated temperature of hot air, K
ΔT_{LMTD}	logarithmic mean temperature difference, K
$\Delta t_{SEP,out}$	temperature difference between the assumed and calculated outlet temperature of SEP, $^{\circ}C$
$\Delta\alpha$	air leakage ratio
δQ_{boiler}	heat difference between the assumed and calculated Q_{boiler} , kJ/kg
ε	hemispherical emittance

η_{boiler}	boiler's thermal efficiency
η_{hel}	heliostat efficiency
η_{solar}	solar thermal-to-electricity efficiency
η_{STACP}	thermal efficiency of STACP system
λ	thermal conductivity of molten salt, W/(m K)
ρ	density of molten salt, kg/m ³
ρ_{CO_2}	density of CO ₂ , kg/m ³
σ_0	Stefan–Boltzmann constant, 5.67×10^{-8} W/(m ² K ⁴)
τ_i	specific enthalpy change of feed-water in the i_{th} heater, kJ/kg
φ	heat retention factor

Mathematical Symbols

A_h	area of heating surface, m ²
A_{hel}	area of a heliostat, m ²
A_r	lateral surface of the tube, m ²
a_{xt}	system emissivity
B_j	calculation coal consumption rate, kg/s
b_s	standard coal consumption rate, kg/kWh
c_p	specific heat of molten salt at constant pressure, J/(kg K)
DNI	direct normal irradiance, W/m ²
Em_{CO_2}	CO ₂ emission, g/kWh
F_{fur}	furnace enclosure wall area, m ²
h_{air}	specific enthalpy of cold air, kJ/kg
$h_{\text{d},i}$	specific enthalpy of drain water in the i_{th} heater, kJ/kg
$h_{\text{flue,in}} (h_{\text{flue,out}})$	specific enthalpy of flue gas in (out) of the heater, kJ/kg
h_i	specific enthalpy of extraction steam for the i_{th} heater, kJ/kg
$h_{\text{mix},i}$	mixed convection coefficient, W/(m ² K)
$h_{\text{ms,in}} (h_{\text{ms,out}})$	specific enthalpy of molten salt in (out) of heat exchanger, kJ/ kg
$h_{\text{wf,in}} (h_{\text{wf,out}})$	specific enthalpy of working fluid in (out) of an equipment, kJ/ kg
$h_{\text{w},i}$	specific enthalpy of feed-water at outlet for the i_{th} heater, kJ/kg
K	heat transfer coefficient
LHV	low heating value of the coal used in this study, kJ/kg
LHV_{st}	low heating value of standard coal, kJ/kg
m_{flue}	mass flow rate of flue gas, kg/s
m_{fw}	mass flow rate of feed-water from deareator, kg/s
m_{ht}	mass of molten salt in hot tank, kg
m_i	mass flow rate of extraction steam in the i_{th} stage, kg/s
m_{ini}	initial mass in hot tank, kg
m_{ms}	mass flow rate of molten salt, kg/s;
$m_{\text{ms,in}} (m_{\text{ms,out}})$	mass flow rate of molten salt in (out) of hot tank, kg/s
m_{wf}	mass flow rate of working fluid, kg/s
Num	number of heliostats
P	net power output of the STACP system, MW
P_{solar}	power produced by solar energy, MW

Q_{add}	assumed heat absorbed by the additional heating surface, kJ/kg
Q_{add}'	calculated heat absorbed by the additional heating surface, kJ/kg
Q_{boiler}	heat absorbed by the working fluid in the boiler, MW
$Q_{boiler,max}$	maximum solar power that can be absorbed by the boiler, MW
Q_{coal}	thermal energy of the coal, MW
Q_{con}	convective heat transferred, kJ/kg
Q_{con}'	calculated convective heat transferred, kJ/kg
Q_{conv}	convection loss of receiver, MW
Q_{de}	heat transferred to the power block at the design point, MW
Q_{fur}	heat absorbed in the furnace, MW
Q_{hel}	solar power reflected by the heliostats, MW
q_i	specific enthalpy drop of extraction steam in i_{th} heater, kJ/kg
Q_{rad}	radiation loss of receiver, MW
$Q_{radiation}$	radiative heat transferred, kJ/kg
Q_{rec}	solar power absorbed by the molten salt in the receiver, MW
$Q_{rec,loss}$	power loss in the receiver, MW
Q_{ref}	power loss reflected from the tube surface, MW
Q_s	solar power falling on the heliostats, MW
$Q_{solar} (Q_{wf})$	power transferred to the water/steam, MW
$QE_{boiler,max}$	maximum solar energy that can be absorbed by the boiler, MWh
QE_{ht}	solar energy stored in the hot tank, MWh
$QE_{ht,loss}$	energy loss of hot tank at t_{int} , MWh
$QE_{in} (QE_{out})$	energy in (out) of hot tank for the t_{int} , MWh
QE_{ini}	initial energy stored in hot tank, MWh
QE_{rec}	solar energy absorbed by the molten salt in the receiver, MWh
T_{ad}	adiabatic flame temperature, K
T_{amb}	ambient air temperature, K
T_b	average temperatures of the furnace wall, K
T_{exg}	temperature of the exit flue gas, K
$T_{flue,in} (T_{flue,out})$	inlet (outlet) temperature of flue gas for a heater,
$t_{FPS,in}$	inlet temperature of FPS, \square
$T_{fur,out}$	temperature at the out of furnace, K
T_{hot}	temperature of hot air, K
T_{hy}	average temperatures of the flame, K
t_{int}	time interval, s
$t_{SEP,out}$	outlet temperature of SEP, \square
$T_{steam,in} (T_{steam,out})$	inlet (outlet) temperature of steam for a heater, K
$T_{wall,i}$	wall temperature, K
VC	mean net heat capacity rate of the combustion products per unit, kJ/(kg K)
V_{CO_2}	volume of CO_2 for the combustion of 1 kg coal, m^3/kg

1. Introduction

In developing countries, coal is still the main energy source to generate electricity at present

[1-3]. With increasing concerns on serious environmental problems caused by coal-fired power plants and fossil resource shortages, it is important to reshape the energy structure and exploit renewable energy to replace the coal. Compared with wind power and photovoltaic, concentrated solar power (CSP) with thermal energy storage can generate stable un-interrupted electricity for different solar radiation condition, which seems to be a promising technology to replace coal as the main power generation technology. However, conventional standalone CSP plants face a lot of difficulties at present, such as the huge investment, lower efficiency compared to fossil fired plants and large scale of thermal energy storage (TES) system requirements, which hinder the large-scale utilisation of solar energy [4, 5]. Integrating solar thermal energy into coal-fired power plant, also known as solar aided coal-fired power (SACP) system, has the potential to reduce the coal consumption in coal-fired power plant and overcome the above mentioned drawbacks of CSP Plants as well [6].

The earliest work of SACP system was conducted by Zoschak and Wu in 1975 [7]. They investigated seven different ways of integrating solar thermal into an 800 MWe coal-fired power plant. Results show that combining solar energy with coal-fired power system is a promising way to use solar energy. The solar-coal hybrid systems are gaining interest in recent years. System integration is the first important problem need to be solved in this area. Hu et al. proposed a SACP system that used solar energy to preheat the feed-water and the results indicated that SACP system is an economical way for solar energy utilisation [8]. Yang et al. considered a 200 MWe coal-fired unit as an example and investigated four different integration schemes, and the results show that the solar thermal to power efficiency can be over 36% for the solar heat at 260 °C [9]. Then, the thermal performance [6, 10-13], economic performance [14, 15] and off-design performance [5, 6, 16] were

studied on the SACP systems. Recently, researchers paid more attention to the optimisation and evaluation method of the SACP system. On the optimisation aspect, Zhao et al. presented an economic benefits of the solar multiple for SACP system with different unit scales [17]. Zhong et al. proposed an operation optimisation strategy for SACP system and applied a mixed-integer nonlinear programming approach to optimise the oil-water heat exchanger area with an optimised operation parameters based on the annual direct normal irradiance (DNI) distribution [18]. Sun et al. optimised the tracking strategy for the parabolic trough collector and results showed there was a boost about 15–17% in collector efficiency [19]. In terms of the evaluation method, Zhai et al. used life cycle assessment method to evaluate the SACP system [20]. Peng et al. applied the energy-utilisation diagram methodology to the SACP system [21]. Hou et al. proposed a new evaluation method of solar contribution in a SACP system based on exergy analysis [22]. Wang et al. evaluated different modes of solar aided coal-fired power generation system through theoretical calculations [23]. These studies indicated that SACP system is a promising way for the large scale utilisation of solar energy with high efficiency and can reduce the fossil fuel load in the coal-fired power system.

Zoschak and Wu's study has showed that integrating solar energy with the evaporation and superheating can achieve more profit than using solar energy to preheat feed-water [7], because the temperature of superheat steam is normally over 500 °C, which is much higher than the temperature of feed-water (lower than 300 °C). Therefore, higher operation temperature of solar field is necessary and solar tower technology is used to assist the coal-fired power system, also known as solar tower aided coal-fired power (STACP) system. STACP system could achieve higher power efficiency than that of traditional SACP system, because solar energy with higher temperature is used in this system. Zhang et al. proposed two schemes of introducing the solar tower with 660 MW_e coal-fired power

plant, and investigated the performance at the design point and the annual performance of the integrated solar tower with a single tank thermocline storage system [5, 24]. Zhu et al. studied the solar tower aided coal-fired power system by performing exergy analysis and techno-economic analysis [25, 26]. Then, the annual performance was investigated and the annual average results show that the reduction of coal consumption rate and the CO₂ emission rate were about 27.3 g/kWh and 10.1% respectively compared with coal-fired power system [1].

Based on authors' detailed literature review, it can be highlighted that the off-design performance study of STACP system is inadequate and the effects of solar multiple (SM) and TES hour are not yet studied. As the solar energy introduced increases, the amount of water/steam exacted from the boiler also increases, thus the amount of heat absorbed and the inlet and outlet temperature of each heater will change as well. When the solar energy increases to a certain extent, it is difficult to maintain the temperature of superheat steam and reheat steam by adjusting the coal consumption rate at the same time. Therefore, the maximum solar energy that the boiler can absorb has to be determined. In our previous study, the STACP system which uses solar tower energy to replace the thermal load of water wall and super-heaters in the boiler has demonstrated better thermal performances than other integration schemes [27]. Therefore, the novelty of this study lies in that: (1) Calculating the maximum solar power that the boiler can absorb ($Q_{\text{boiler,max}}$) for the above mentioned STACP system at 100% load, 75% load, and 50% load. (2) Exploring the thermal performance of the STACP system with different solar energy shares for the selected loads. (3) The impacts of SM and TES hour on the daily performance of STACP.

2. System description

2.1 Solar tower aided coal-fired power system

Fig. 1 shows a schematic diagram of the STACP system, which is composed of the “solar part” and the “coal-fired part”. The “solar part” contains heliostats, a solar tower, a columnar receiver, the TES system and a heat exchanger. The solar energy is reflected onto a receiver by the heliostats. After absorbing the solar energy in the receiver, the hot molten salt flows into the hot tank. According to the operation strategy of STACP system, the flow rate of the molten salt out of the hot tank can be adjusted. After releasing thermal energy to the steam/water in the molten salt heat exchanger (MSHE), molten salt flows into and stores in the cold tank. Then the cold molten salt is pumped to the receiver for further solar energy collection. The molten salt used is a mixture of 60 % NaNO₃ and 40 % KNO₃ and the properties of the molten salt are as follows [28]:

$$\rho=2263.72-0.636T \quad (1)$$

$$c_p=1396.02+0.172T \quad (2)$$

$$\lambda=0.391+0.00019T \quad (3)$$

Where ρ is the density of molten salt; c_p is the specific heat of molten salt at constant pressure; λ is the thermal conductivity of molten salt; T is the temperature of molten salt.

In this study, we consider a supercritical coal-fired power plant which is based on single-reheat and condensing steam turbines arrangement with rated capacity of 600 MW_e at the design point. The thermal parameters of the main steam and reheat steam are 566/24.2 and 566/3.6 (□/MPa), respectively.

In the “coal-fired part”, the unsaturated feed-water from the condenser enters into the boiler after going through condensate pump, four low pressure heaters (H5, H6, H7, and H8), a deaerator (H4), feed-water pump and three high pressure heaters (H1, H2, and H3). Feed-water from the high pressure heaters first goes to the economizer (ECO). The water out from the ECO is divided into

two parts. One part flows into the heat exchange to absorb solar energy in the “solar part”. The other part flows into the water wall from the bottom of the boiler, where the water partially turns into steam due to the radiative heat absorption from the furnace flame. Then the steam/water mixture enters to the steam separator (SEP), where the steam is separated and passes through first platen super-heater (FPS), second platen super-heater (SPS) and final super-heater (FS). Then, the superheat steam mixes with the steam from the “solar part” and enters to the high pressure turbine (HP) to produce power. Later, the steam out from HP returns back to the boiler to be reheated in the low-temperature re-heater (LR) and high temperature re-heater (HR) to improve the work capacity and efficiency by increasing the average heat addition temperature. Then, the reheat steam is transported to the intermediate pressure turbine (IP) and the low pressure turbine (LP) to produce further electric power, finally exhaust steam is condensed in the condenser.

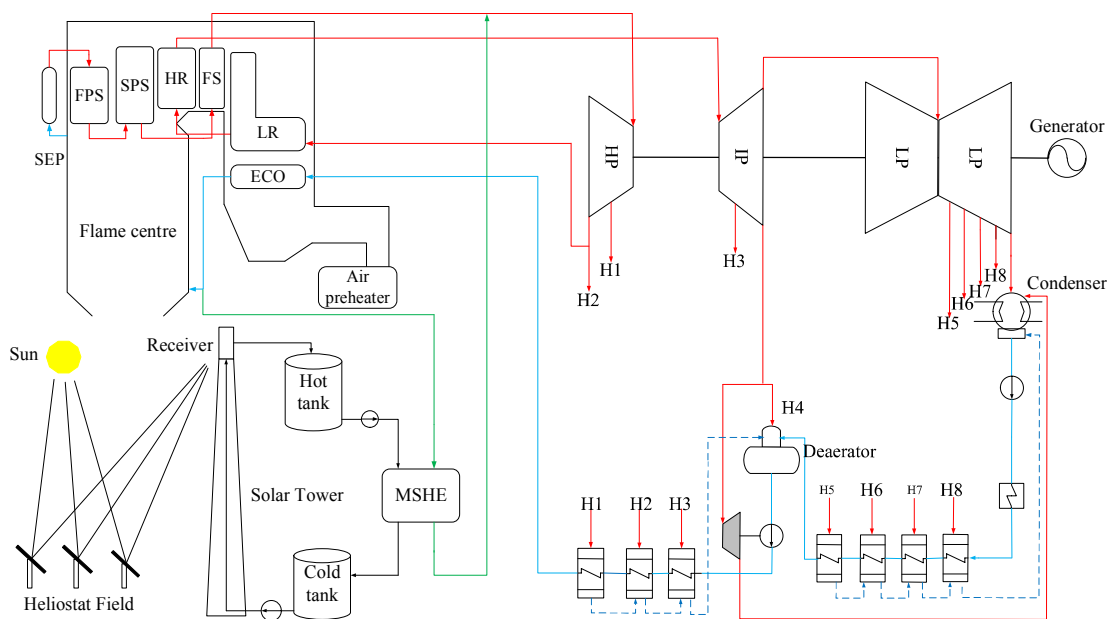


Fig.1 The diagram of solar aided coal-fired power system (red line: steam; blue line: water; green line: extracted water/steam)

2.2 Operational Strategies

The operation strategies of the STACP system with thermal storage system are mainly

dependent on the relationship between solar energy collected by the receiver (QE_{rec}), solar energy stored in the hot tank (QE_{ht}) and maximum solar energy that can be absorbed by the boiler ($QE_{boiler,max}$), and the following six conditions are defined as:

(1) When $QE_{rec} \geq QE_{boiler,max}$, the solar energy absorbed by the boiler is $QE_{boiler,max}$ and the extra solar energy is stored in the hot tank.

(2) When $QE_{rec} < QE_{boiler,max}$, and $QE_{ht} \geq QE_{boiler,max} - QE_{rec}$, the solar energy absorbed by the boiler is $QE_{boiler,max}$.

(3) When $QE_{rec} < QE_{boiler,max}$, and $QE_{ht} < QE_{boiler,max} - QE_{rec}$, the solar energy absorbed by the boiler is $QE_{rec} + QE_{ht}$.

(4) When $QE_{rec} = 0$, and $QE_{ht} \geq QE_{boiler,max}$, the solar energy absorbed by the boiler is $QE_{boiler,max}$.

(5) When $QE_{rec} = 0$, and $QE_{ht} < QE_{boiler,max}$, the solar energy absorbed by the boiler is QE_{ht} .

(6) When $QE_{rec} = 0$, and $QE_{ht} = 0$, the solar energy absorbed by the boiler is 0. The STACP system operates in the standalone coal-fired power generation mode.

3. Modeling Methodology

3.1 Heliostat field

Heliostat field consists of plenty of heliostats, which can reflect sun rays to the receiver at the top of the solar tower. The thermal power reflected to the receiver can be calculated as:

$$Q_{hel} = Q_s \cdot \eta_{hel} \quad (4)$$

Where, Q_{hel} is the solar power reflected by the heliostats. η_{hel} is the heliostat efficiency, which can be expressed by mirror reflectivity, cosine factor, atmospheric attenuation factor, shading and blocking factor and interception factor. The calculation method of heliostat efficiency and the

validation of the heliostat model can be found in literature [29, 30]. Q_s is the solar power falling on the heliostats and can be calculated by:

$$Q_s = \text{Num} \cdot A_{\text{hel}} \cdot \text{DNI} / 10^6 \quad (5)$$

Where, Num is the number of heliostats; A_{hel} is the area of a heliostat.

3.2 Receiver

The temperature of molten salt increases, when it passes through the receiver which is at the top of the solar tower. The energy balance for the receiver is as follows:

$$Q_{\text{rec}} = Q_{\text{hel}} - Q_{\text{rec,loss}} \quad (6)$$

$$Q_{\text{rec,loss}} = Q_{\text{ref}} + Q_{\text{rad}} + Q_{\text{conv}} \quad (7)$$

Where, Q_{rec} is thermal power absorbed by the molten salt in the receiver; $Q_{\text{rec,loss}}$ is the thermal power loss in the receiver; Q_{ref} is the thermal power loss reflected from the tube surface; Q_{rad} is the radiation loss of receiver; Q_{conv} is the convection loss of receiver. Q_{ref} , Q_{rad} and Q_{conv} can be obtained by [31].

$$Q_{\text{ref}} = (1 - \alpha) Q_{\text{hel}} \quad (8)$$

$$Q_{\text{rad}} = \sum \varepsilon \sigma_0 A_r (T_{\text{wall},i}^4 - T_{\text{amb}}^4) \quad (9)$$

$$Q_{\text{conv}} = \sum h_{\text{mix},i} A_r (T_{\text{wall},i} - T_{\text{amb}}) \quad (10)$$

Where, α is concerning solar absorptance of the tube panels; ε is hemispherical emittance; σ_0 is Stefan–Boltzmann constant, $5.67 \times 10^{-8} \text{ W}/(\text{m}^2\text{K}^4)$; A_r is lateral surface of the tube; $h_{\text{mix},i}$ is mixed convection coefficient; $T_{\text{wall},i}$ is the wall temperature; T_{amb} is ambient air temperature. The receiver model is validated with data from Solar Two power plant [31, 32]. The theoretical efficiency of the receiver is 87.36%, which agrees well with the test data demonstrated as 86-88% [32]. Similarly, the other researchers quoted the receiver efficiency as 78-88% by Lata et al. [33] and 83-90% by

Jianfeng et al. [34]. Therefore, the calculated results of this model are reasonable, which means that our model is reliable.

3.3 Thermal energy storage system

The thermal storage system is of the typical two-tank type, which uses molten salt as the storage media. In this study, the TES system is assumed to operate at a steady state for an hour. The mass balance and energy balance for these two tanks are similar. Take the hot tank as an example.

$$m_{ht} = m_{ini} + (m_{ms,in} - m_{ms,out})t_{int} \quad (11)$$

$$QE_{ht} = QE_{ini} + QE_{in} - QE_{out} - QE_{ht,loss} \quad (12)$$

Where, m_{ht} is the mass of molten salt in hot tank; m_{ini} is initial mass in hot tank; $m_{ms,in}$ and $m_{ms,out}$ are the inlet/outlet mass flow rate of molten salt of hot tank; t_{int} is time interval; QE_{ini} is initial energy stored in hot tank; QE_{in} and QE_{out} are the energy in/out of hot tank for the t_{int} ; $QE_{ht,loss}$ is energy loss at t_{int} and is neglected in this study.

3.4 Molten salt heat exchanger

The energy balance of the heat exchanger can be expressed as:

$$Q_{solar} = 10^{-3} m_{ms} (h_{ms,out} - h_{ms,in}) \quad (13)$$

$$Q_{wf} = 10^{-3} m_{wf} (h_{wf,out} - h_{wf,in}) \quad (14)$$

Where, Q_{solar} and Q_{wf} are both the power transferred to the water/steam; m_{ms} is the mass flow rate of molten salt; $h_{ms,in}$ and $h_{ms,out}$ are the specific enthalpy of molten salt in/out of heat exchanger respectively. m_{wf} is the mass flow rate of working fluid (water/steam); $h_{wf,in}$ and $h_{wf,out}$ are the specific enthalpy of working fluid in/out of heat exchanger respectively.

3.5 Boiler

Boiler model is established based on the principle that was proposed by the former Soviet

Union in 1973 and was modified in China in 1998 [35]. The calculation logical flow diagram for the boiler is shown in Fig. 2.

In furnace, radiative heat transfer is predominant and the convection heat transfer can be ignored [35]. According to energy conservation principle, the heat absorption from the flue gas in the furnace can be considered to be equal to the enthalpy drop from the adiabatic flame temperature to the temperature at the out of furnace. Therefore, the basic equation for furnace heat transfer calculation is as follows:

$$Q_{\text{fur}}=10^{-3}\varphi B_j VC(T_{\text{ad}}-T_{\text{fur,out}})=10^{-6}a_{\text{xt}}F_{\text{fur}}\sigma_0(T_{\text{hy}}^4-T_{\text{b}}^4) \quad (15)$$

Where, Q_{fur} is the heat absorbed in the furnace; φ is heat retention factor; B_j is calculation coal consumption rate; VC is mean net heat capacity rate of the combustion products per unit; T_{ad} is adiabatic flame temperature; $T_{\text{fur,out}}$ is the temperature at the out of furnace; a_{xt} is system emissivity; F_{fur} is furnace enclosure wall area; T_{hy} and T_{b} are average temperatures of the flame and the furnace wall respectively.

The convective heating surfaces refer to all the heating surfaces in the flue gas pass beyond furnace outlet. The calculation logic flow for each heater is shown in Fig. 3. The heat balance equations for the convective heating surface are as follows:

$$Q_{\text{con}}=\frac{KA_h\Delta T_{\text{LMTD}}}{B_j} \quad (16)$$

For gas side:

$$Q_{\text{con}}=\varphi(h_{\text{flue,in}}-h_{\text{flue,out}}+\Delta\alpha h_{\text{air}}) \quad (17)$$

For working fluid side:

$$Q_{\text{con}}=\frac{m_{\text{wf}}(h_{\text{wf,out}}-h_{\text{wf,in}})}{B_j}-Q_{\text{radiation}} \quad (18)$$

Where, Q_{con} is convective heat transferred; K is heat transfer coefficient; A_h is the area of heating

surface; ΔT_{LMTD} is the logarithmic mean temperature difference; $h_{flue,in}$ and $h_{flue,out}$ are the specific enthalpy of flue gas in/out of the heater; $\Delta\alpha$ is the air leakage ratio; h_{air} is the specific enthalpy of cold air; m_{wf} is the mass flow rate of steam/water; $h_{wf,in}$ and $h_{wf,out}$ are the specific enthalpy of steam in/out of the heater respectively; $Q_{radiation}$ is radiative heat transferred.

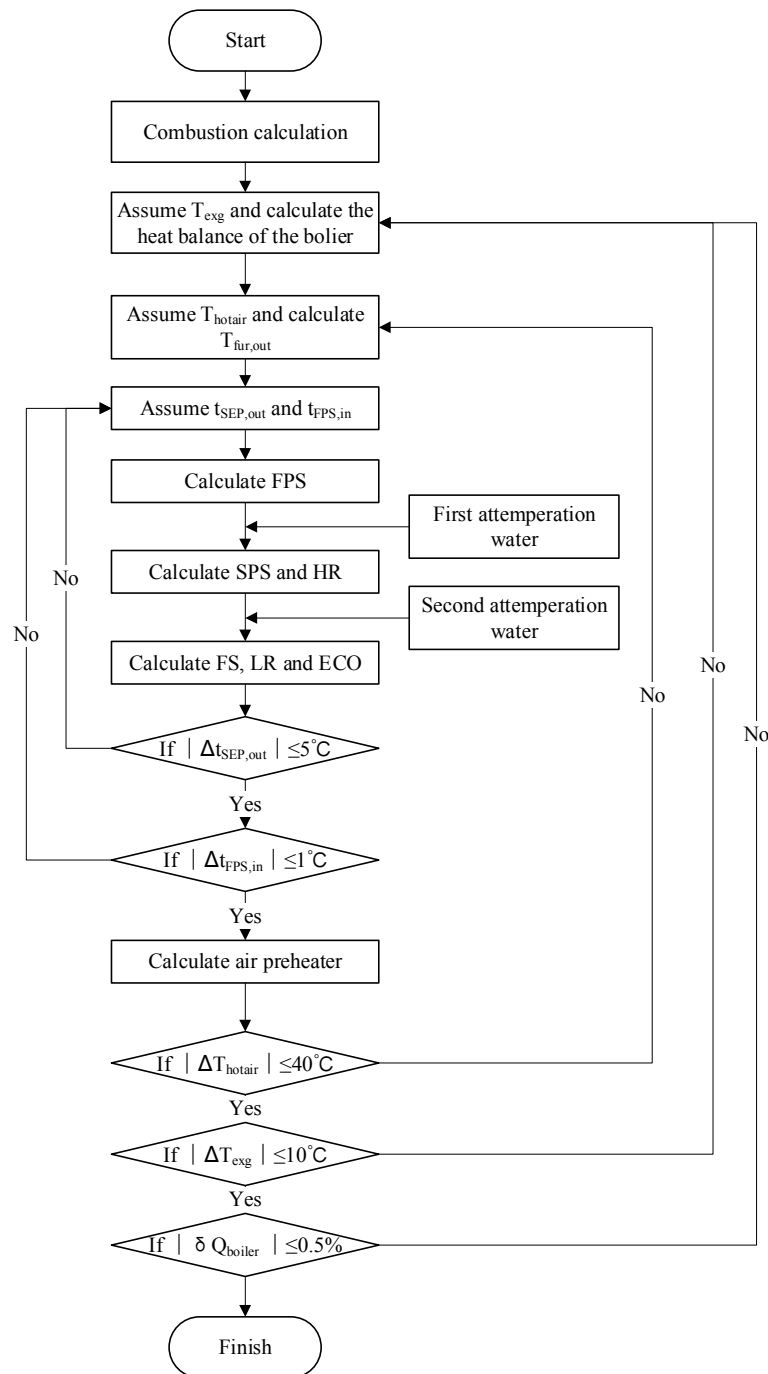


Fig. 2 Calculation logic flow of the boiler model

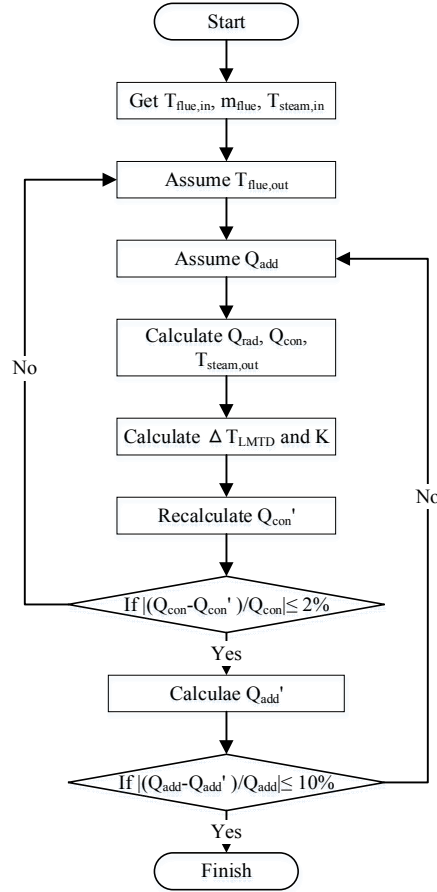


Fig. 3 The calculation logic flow for each heater

3.6 Turbine and feed-water preheating system

In this study, the energy balance matrix used to calculate turbine and feed-water preheating system can be expressed as:

$$\begin{bmatrix}
 q_1 \\
 \gamma_2 & q_2 \\
 \gamma_3 & \gamma_3 & q_3 \\
 \gamma_4 & \gamma_4 & \gamma_4 & q_4 \\
 \tau_5 & \tau_5 & \tau_5 & \tau_5 & q_5 \\
 \tau_6 & \tau_6 & \tau_6 & \tau_6 & \gamma_6 & q_6 \\
 \tau_7 & \tau_7 & \tau_7 & \tau_7 & \gamma_7 & \gamma_7 & q_7 \\
 \tau_8 & \tau_8 & \tau_8 & \tau_8 & \gamma_8 & \gamma_8 & \gamma_8 & q_8
 \end{bmatrix}
 \begin{bmatrix}
 m_1 \\
 m_2 \\
 m_3 \\
 m_4 \\
 m_5 \\
 m_6 \\
 m_7 \\
 m_8
 \end{bmatrix}
 = m_{fw}
 \begin{bmatrix}
 \tau_1 \\
 \tau_2 \\
 \tau_3 \\
 \tau_4 \\
 \tau_5 \\
 \tau_6 \\
 \tau_7 \\
 \tau_8
 \end{bmatrix}
 \quad (19)$$

Where, m_{fw} is mass flow rate of feed-water from deareator; m_i is mass flow rate of extraction steam in the i_{th} stage; τ_i is the specific enthalpy change of feed-water in the i_{th} heater; q_i is specific enthalpy drop of extraction steam in i_{th} heater; γ_i is specific enthalpy drop of drain water in the i_{th} heater.

q , γ , τ can be obtained as follows:

$$q_i = \begin{cases} h_i - h_{d,i} & (i=1,2,3,5,6,7,8) \\ h_i - h_{w,5} & (i=4) \end{cases} \quad (20)$$

$$\tau_i = h_{w,i} - h_{w,i+1} \quad (21)$$

$$\gamma_i = \begin{cases} h_{d,i-1} - h_{d,i} & (i=2,3,6,7,8) \\ h_{d,3} - h_{w,5} & (i=4) \end{cases} \quad (22)$$

Where, h_i is the specific enthalpy of extraction steam for the i_{th} heater; $h_{w,i}$ is the specific enthalpy of feed-water at outlet for the i_{th} heater; $h_{d,i}$ is the specific enthalpy of drain water in the i_{th} heater.

3.7 Model validation

In this study, a 600 MW_e coal-fired power plant in China is selected as the reference system and the boiler model and turbine and preheating system model are coded in MATLAB. The off-design and simulation values of 100% load, 75% load and 50% load of boiler are shown in Table 1 while the turbine and preheating system are shown in Table 2. From Table 1 and Table 2, a strong agreement can be seen between the simulation results and the design data. Thus, our model developed in MATLAB is reliable enough to use for further analysis.

Table 1 Off-design and simulation values of 100% load, 75% load and 50% load of the boiler

Parameter	Units	Working Fluid			
		Inlet		Outlet	
		design	simulation*	design	simulation*
100% load (design)					
First Platen Super-heater	□	428	429.5	470	470.5
Second Platen Super-heater	□	460	461.6	512	509.6
High-temperature Re-heater	□	468	469.5	566	567.0
Final Super-heater	□	504	505.9	566	571.0
Low-temperature Re-heater	□	300	300.0	468	469.5
Economizer	□	274	274.0	329	330.9
Air Heater	□	25	25.0	325	323.0
75% load					
First Platen Super-heater	□	419	419.0	465	464.6
Second Platen Super-heater	□	454	454.2	510	509.5
High-temperature Re-heater	□	467	466.6	566	566.0
Final Super-heater	□	501	501.6	566	566.0
Low-temperature Re-heater	□	282	282.0	467	466.6

Economizer	□	255	255.0	318	316.3
Air Heater	□	25	25.0	305	300.2
50% load					
First Platen Super-heater	□	376	375.9	443	442.0
Second Platen Super-heater	□	425	425.2	504	503.1
High-temperature Re-heater	□	466	466.5	566	566.0
Final Super-heater	□	495	495.6	566	566.0
Low-temperature Re-heater	□	291	291.0	466	466.5
Economizer	□	232	232.0	299	298.3
Air Heater	□	25	25.0	280	275.3

* The data are calculated without any solar energy input.

Table 2 Off-design and simulation values of 100% load, 75% load and 50% load of turbine and preheating system

Parameter	Pressure (MPa)	Enthalpy (kJ/kg)		Flow rate (t/h)	
		design	simulation*	design	simulation*
100% load (design)					
Main steam	24.2	3396	3398.8	1677.539	1677.54
Cold reheat steam	4.047	2970.1	2968.5	1400.299	1403.55
Hot reheat steam	3.642	3598.3	3600.0	1400.299	1403.55
1st extraction	5.977	3054.8	3051.8	104.233	105.59
2nd extraction	4.047	2970.1	2968.5	145.786	141.74
3rd extraction	1.774	3376.2	3376.5	60.875	62.00
4th extraction	0.9513	3189.1	3188.8	78.858	79.65
5th extraction	0.372	2974.9	2974.9	82.503	82.17
6th extraction	0.113	2733.8	2734.1	40.636	40.68
7th extraction	0.05577	2621.1	2621.1	54.609	54.68
8th extraction	0.0178	2493.7	2493.7	35.538	36.31
Exhaust steam	0.00588	2361.5	2361.5	973.83	975.24
75% load					
Main steam	24.2	3396.0	3398.8	1222.12	1222.12
Cold reheat steam	3.015	2955.2	2955.2	1038.299	1039.46
Hot reheat steam	2.714	3607.8	3608.3	1038.299	1039.46
1st extraction	4.387	3035.2	3035.3	65.459	65.53
2nd extraction	3.015	2955.2	2956.2	96.985	96.84
3rd extraction	1.37	3384.5	3386.5	41.207	44.01
4th extraction	0.7192	3198.5	3198.2	54.576	58.60
5th extraction	0.2978	2984.0	2984.0	57.734	57.48
6th extraction	0.09027	2741.0	2741.0	28.61	28.68
7th extraction	0.04466	2630.8	2630.8	38.657	38.68
8th extraction	0.01438	2498.8	2498.8	18.282	19.84
Exhaust steam	0.00588	2398.6	2398.6	751.045	751.09
50% load					
Main steam	16.497	3475.9	3478.6	798.525	798.53
Cold reheat steam	2.028	2993.4	2992.9	693.435	692.85

Hot reheat steam	1.825	3614.8	3616.1	693.435	692.85
1st extraction	2.96	3077.9	3076.42	36.186	36.62
2nd extraction	2.028	2993.4	2992.9	54.066	55.61
3rd extraction	0.931	3395.5	3395.9	25.078	23.90
4th extraction	0.499	3214.0	3214.0	33.518	35.20
5th extraction	0.208	2999.4	2999.4	35.756	35.66
6th extraction	0.06283	2753.1	2753.2	17.827	17.91
7th extraction	0.03118	2638.3	2638.4	24.254	24.37
8th extraction	0.01015	2506.2	2506.2	4.972	5.67
Exhaust steam	0.00588	2458.4	2458.4	533.312	534.41

* The data are calculated without any solar energy input.

3.8 Thermodynamic parameters

Solar multiple is an important parameter for the solar thermal power plant, which is the ratio of heat absorbed by the molten salt in the receiver to that transferred to the power block at the design point (Q_{de}).

It can be obtained by [1]:

$$SM = \frac{Q_{rec}}{Q_{de}} \quad (23)$$

The thermal efficiency of STACP system can be expressed:

$$\eta_{STACP} = \frac{P}{Q_{coal} + Q_{solar}} \quad (24)$$

Where, P is the net power output of the STACP system; Q_{coal} is the thermal energy of the coal.

Boiler's thermal efficiency can be obtained by:

$$\eta_{boiler} = \frac{Q_{boiler}}{Q_{coal}} \quad (25)$$

Where, Q_{boiler} is the heat absorbed by the working fluid in the boiler.

Standard coal consumption rate can be obtained by:

$$b_s = \frac{3.6 \times 10^6 Q_{coal}}{LHV_{st} P} \quad (26)$$

Where, LHV_{st} is the low heating value of standard coal, which is 29271 kJ/kg.

The CO₂ emissions can be calculated by:

$$Em_{CO_2} = \frac{3.6 \times 10^6 V_{CO_2} P_{CO_2} Q_{coal}}{LHV \cdot P} \quad (27)$$

Where, Em_{CO_2} is the CO₂ emission; V_{CO_2} is the volume of CO₂ for the combustion of 1 kg coal

[35]; ρ_{CO_2} is the density of CO_2 ; LHV is the low heating value of the coal used in this study.

Solar thermal-to-electricity efficiency can be obtained by:

$$\eta_{\text{solar}} = \frac{P_{\text{solar}}}{Q_{\text{solar}}} \quad (28)$$

Where, P_{solar} is the power produced by solar energy. In this study, for a particular load, solar energy is introduced into the boiler and the mass flow rate of superheat steam and reheat steam do not change.

Therefore, the power produced by solar energy cannot be obtained easily by the cycle efficiency of the power block. The calculation method of P_{solar} used in this study has been calculated from literature [24].

4. Case study-results and discussions

4.1 Input conditions

In this study, the STACP system is considered at Lhasa (29.67° N, 91.13° E) and the design point of the heliostat field is set as the solar noon on the summer solstice (21st June). The parameters of heliostat field are shown on Table 3. The DNI values for spring equinox, summer solstice, autumnal equinox and winter solstice are presented in Fig. 4. The temperature of hot tank and cold tank are assumed to be 580 °C and 350 °C. The daily performance is calculated from the time when the solar field starts to work and lasts for 24 hours. The heliostat field starts to work, when the solar altitude angle is higher than 15°. The time of the heliostat starting to work on spring equinox, summer solstice, autumnal equinox and winter solstice are 8:00 AM, 7:00 AM, 8:00 AM and 9:00 AM, respectively.

Table 3 Parameters of the solar field

Parameter	Value	Unit
Tower height	140	m
Receiver radius	4	m
Receiver height	9	m
Heliostat total height	9.75	m
Heliostat total width	12.305	m
Heliostat pedestal height	5	m
Standard deviation surface error	0.94	mrad

Standard deviation tracking error	0.63	mrاد
Standard deviation of sunshape	2.51	mrاد
Heliostat effective reflectivity	0.836	-
Concerning solar absorptance	0.95	-
Total hemispherical emittance	0.88	-

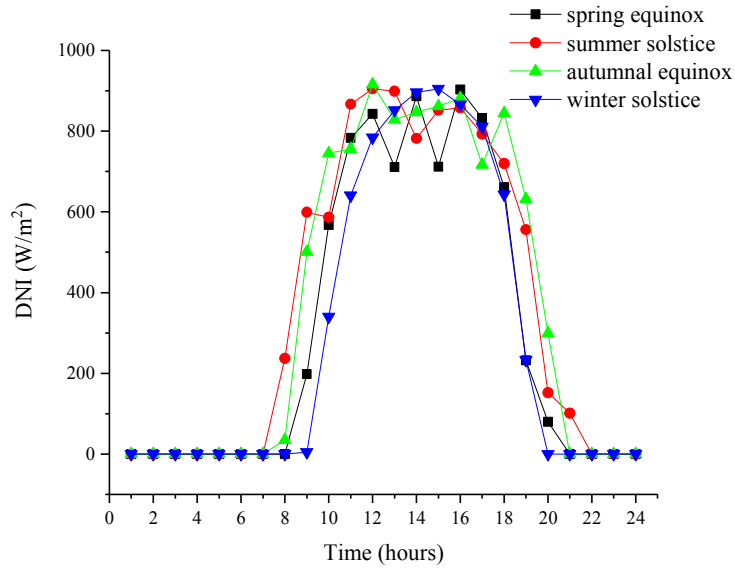


Fig. 4 DNI values during the spring equinox, summer solstice, autumnal equinox, and winter solstice

The properties of the bituminous coal are shown in Table 4.

Table 4 Properties of the coal

Items	Value
Ultimate analysis (%)	
Ash	23.72
Moisture	25
Carbon	57.5
Hydrogen	3.11
Nitrogen	0.99
Sulfur	2
Oxygen	2.78
Low heating value (kJ/kg)	21981

4.2 Effects of solar load on the boiler

In this section, effects of different solar shares introduced to the boiler under different loads are investigated. Fig. 5 represents the effects of solar load on the standard coal consumption rate. From the figure, while keeping the parameters of superheat steam and reheat steam unchanged, the maximum solar power that boiler can absorb at 100% load, 75% load and 50% load are 76.4 MW_{th},

54.2 MW_{th} and 23.0 MW_{th}, respectively. Considering the real-time power loads from a coal-fired power plant in China over a year averaged up to 90% load most of the time (shown in Appendix A), the design heat load of the solar field in STACP system is set as 68.8 MW_{th} (for 100% load shown as 76.4 MW_{th}). The standard coal consumption rate and CO₂ emissions both show a downward trend with the increase in solar energy. For 100% load, when the solar energy increases from 0 MW_{th} to 76.4 MW_{th}, the standard coal consumption rate decreases from 273.84 g/kWh to 260.31 g/kWh and the CO₂ emissions decline from 774.70 g/kWh to 736.42 g/kWh. For 75% load, when the solar energy increases from 0 MW_{th} to 54.2 MW_{th}, the standard coal consumption rate decreases from 284.73 g/kWh to 271.92 g/kWh and the CO₂ emissions decline from 805.51 g/kWh to 769.26 g/kWh. For 50% load, when the solar energy increases from 0 MW_{th} to 23.0 MW_{th}, the standard coal consumption rate declines from 300.40 g/kWh to 292.18 g/kWh and the CO₂ emissions decline from 849.82 g/kWh to 826.57 g/kWh. The maximum saved standard coal consumption rate at 100% load, 75% load and 50% load are 13.53 g/kWh, 12.81 g/kWh and 8.22 g/kWh, respectively.

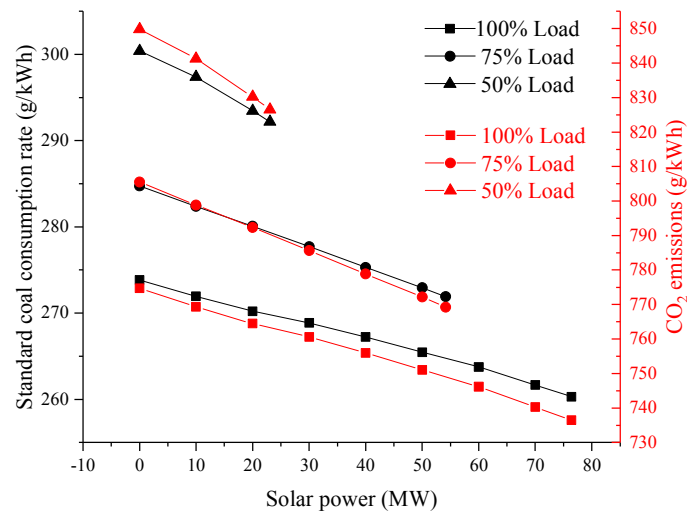


Fig. 5 Effects of solar energy on standard coal consumption rate and CO₂ emissions

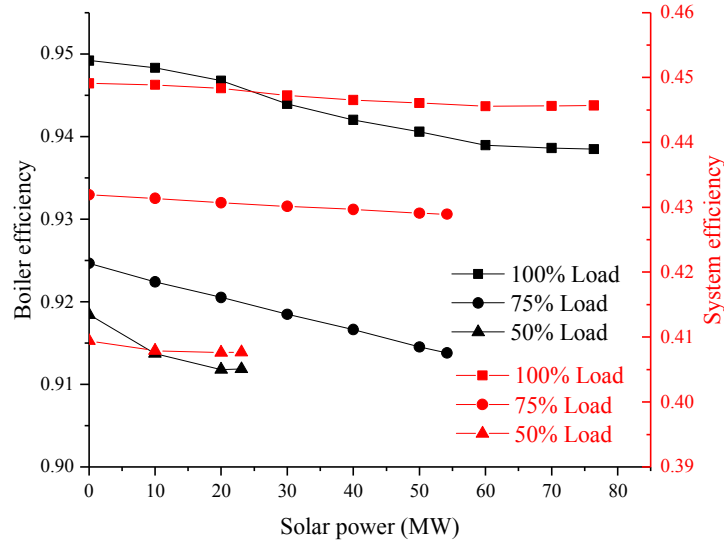


Fig. 6 Effects of solar energy on boiler and system efficiencies

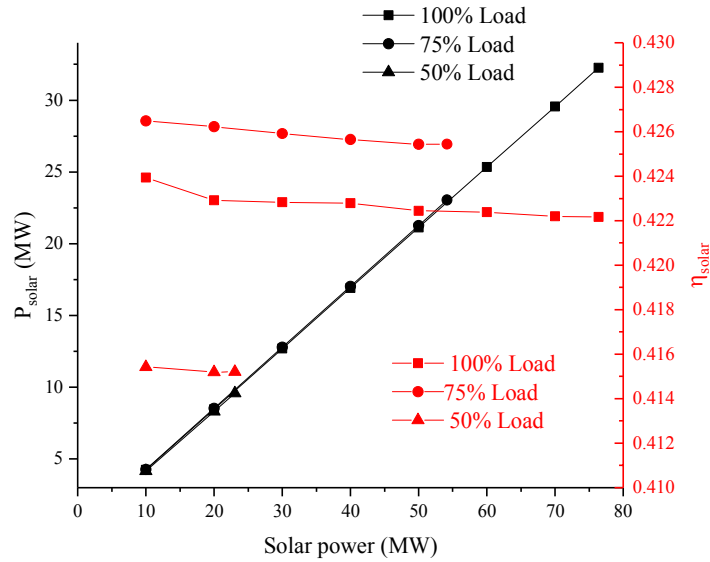


Fig. 7 Effects of solar energy on solar generating power and solar thermal-to-power efficiency

Fig. 6 shows the effects of solar power on boiler and system efficiencies. From the figure, for 100% load, when the Q_{solar} changes between 0 MW_{th} and 76.4 MW_{th} , the boiler efficiency declines from 94.92% to 93.85%; the system efficiency slightly decreases from 44.91% to 44.57%. For 75% load, when the Q_{solar} changes between 0 MW_{th} and 54.2 MW_{th} , the boiler efficiency declines from 92.47% to 91.38%; the system efficiency slightly decreases from 43.19% to 42.89%. For 50% load, when the Q_{solar} changes between 0 MW_{th} and 23.0 MW_{th} , the boiler efficiency declines from 91.84% to 91.18%; the system efficiency slightly decreases from 40.94% to 40.76%. Fig. 7 shows the effects

of solar energy on solar generating power and solar thermal-to-power efficiency. With the increase of Q_{solar} , the P_{solar} shows an increase trend, while the η_{solar} shows a downward trend. Interestingly, the slope of P_{solar} for three different loads are almost equal for the change in Q_{solar} . Take $20 \text{ MW}_{\text{th}}$ as an example, the P_{solar} for 100% load, 75% load and 50% load are $8.46 \text{ MW}_{\text{th}}$, $8.52 \text{ MW}_{\text{th}}$ and $8.30 \text{ MW}_{\text{th}}$, respectively. In addition, the η_{solar} of 75% load is the highest (about 42.6%), while the η_{solar} of 50% load is the lowest (about 41.5%). The solar efficiency for 75% load is higher than 100% load while keeping the main stream conditions same due to extraction pressure is lower for 75% load.

4.3 Effects of solar multiple and thermal energy storage hour

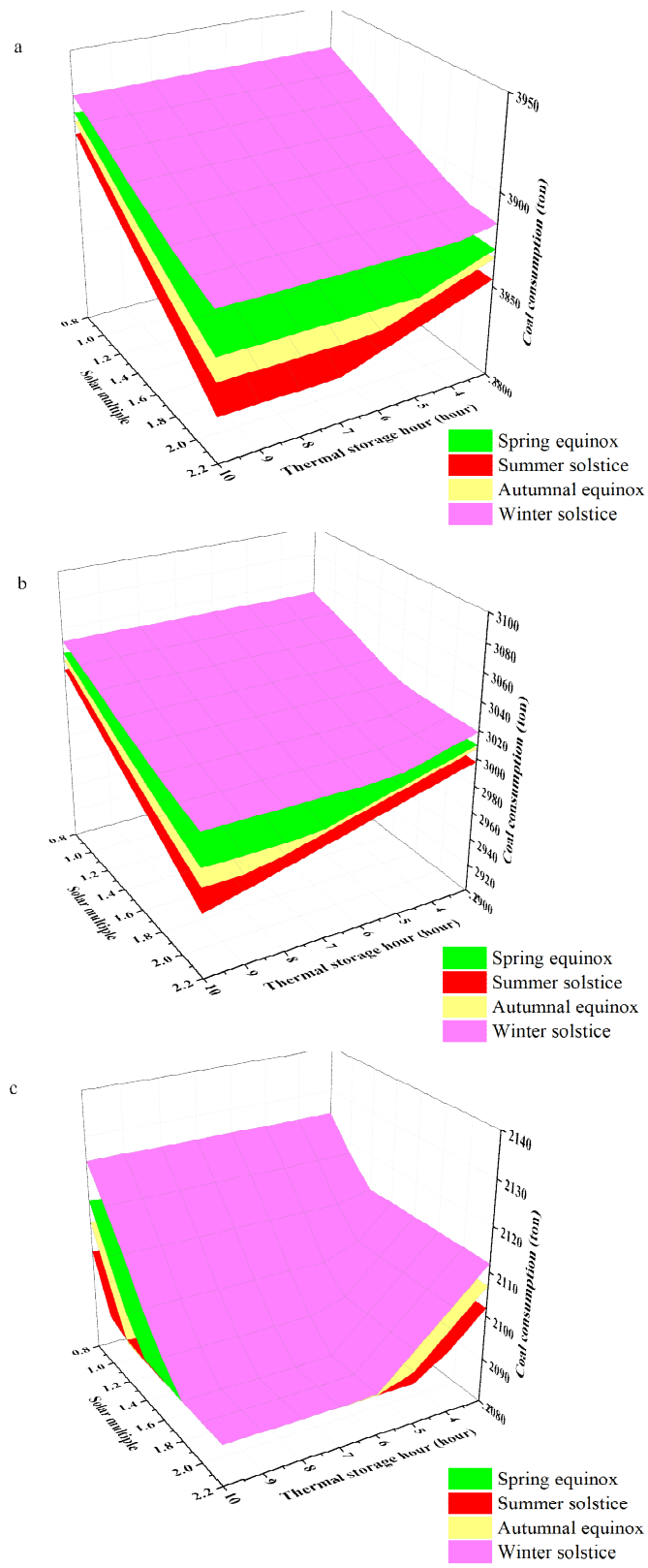


Fig. 8 Effects of solar multiple and TES hour on daily standard coal consumption at (a)100% load, (b)75% load and (c)50% load

It is shown from Fig. 8 that summer solstice has the lowest daily standard coal consumption and winter solstice has the highest daily standard coal consumption with the same SM and TES hour.

This is due to the available solar energy on summer solstice is highest while the available solar energy on winter solstice is lowest. Table 5 shows the highest and lowest daily standard coal consumption and the requirements to reach minimal daily coal consumption. For 100 % load, when the SM is 2.2 and the TES hours of spring equinox, summer solstice, autumnal equinox and winter solstice are longer than 5 hours, 8 hours, 7 hours and 4 hours respectively to reach the minimal daily coal consumption. This means that SM is the factor that limits the further decline of coal consumption. If SM increases, more coal should be saved further per day. The differences between the highest and lowest coal consumption of spring equinox, summer solstice, autumnal equinox and winter solstice are 61.67 ton, 81.16 ton, 69.98 ton and 46.62 ton, respectively. It indicates it can achieve more profit on summer solstice than that on other typical days with the increase in SM and TES hour. For 75 % load, the differences between the highest and lowest coal consumption of spring equinox, summer solstice, autumnal equinox and winter solstice are 63.21 ton, 83.06 ton, 71.62 ton and 47.71 ton, respectively. For 50% load, these four typical days have the same lowest daily coal consumption (2089.33 ton), which means that the STACP system can operate on the hybrid mode with the maximum solar energy introduced for 24 hours when the requirements are met in Table 5. The differences between the highest and lowest coal consumption of spring equinox, summer solstice, autumnal equinox and winter solstice are 26.06 ton, 14.17 ton, 21.17 ton and 35.21 ton, respectively. Summer solstice has the lowest difference, because more solar energy can be used on summer solstice and the reduced coal consumption of summer solstice is higher than that of other three days when SM is 0.8 and TES hour is 3 hours.

Table 5. Results of effects of solar multiple and TES hour on daily standard coal consumption

Loads	Typical day	Highest coal consumption (ton)	Lowest coal consumption (ton)	Requirements
-------	-------------	--------------------------------	-------------------------------	--------------

100% Load	Spring equinox	3917.73	3855.97	SM=2.2 & TES hour \geq 5 h
	Summer solstice	3906.32	3825.16	SM=2.2 & TES hour \geq 8 h
	Autumnal equinox	3913.03	3843.05	SM=2.2 & TES hour \geq 7 h
	Winter solstice	3926.52	3879.90	SM=2.2 & TES hour \geq 4 h
75% Load	Spring equinox	3041.52	2978.31	SM=2.2 & TES hour \geq 8 h
	Summer solstice	3029.84	2946.78	SM=2.2 & TES hour=10 h
	Autumnal equinox	3036.71	2965.09	SM=2.2 & TES hour \geq 9 h
	Winter solstice	3050.51	3002.80	SM=2.2 & TES hour \geq 6 h
50 % Load	Spring equinox	2115.39	2089.33	SM \geq 1.8 & TES hour \geq 6 h
	Summer solstice	2103.50	2089.33	SM \geq 1.6 & TES hour \geq 5 h
	Autumnal equinox	2110.49	2089.33	SM \geq 1.2 & TES hour \geq 6 h
	Winter solstice	2124.54	2089.33	SM \geq 1.8 & TES hour \geq 7 h

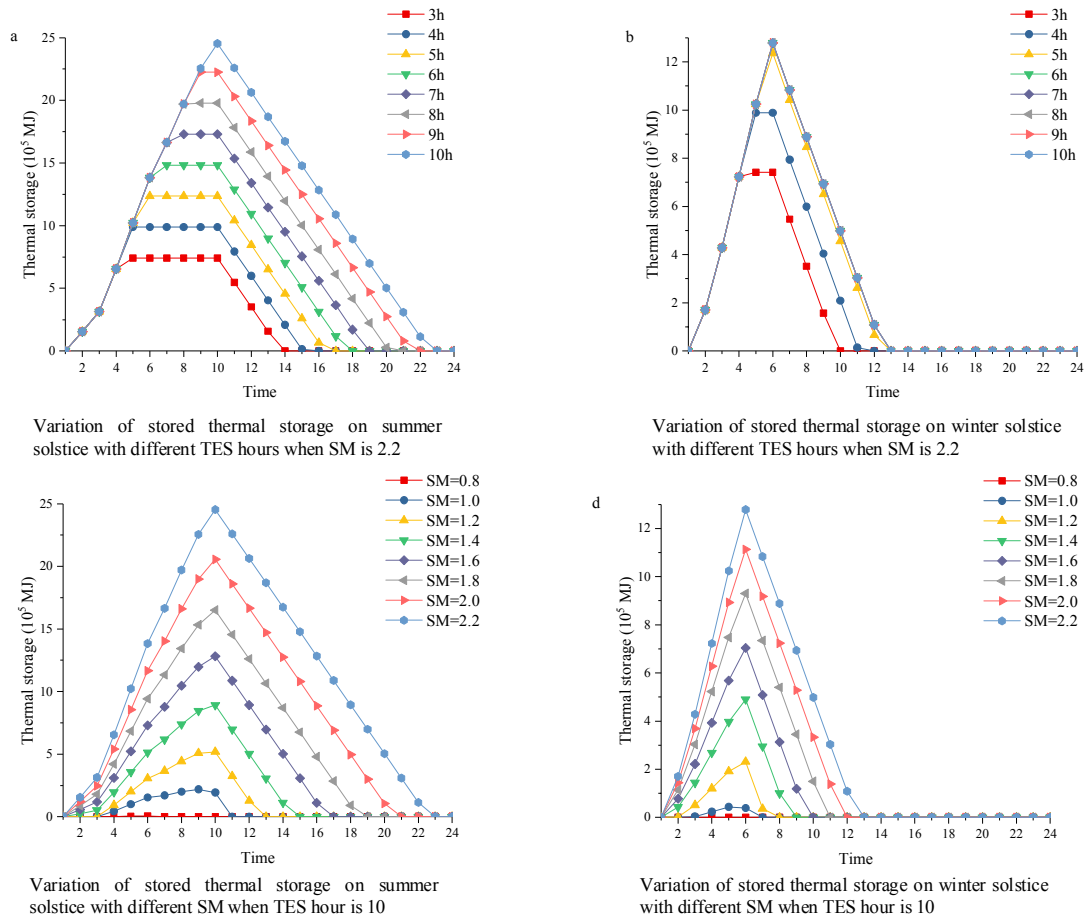


Fig. 9 Effects of solar multiple and TES hour on thermal storage (75% load)

For example, 75% load scenario, the effects of SM and TES hour on the stored thermal energy throughout a day is shown in Fig.9. Fig. 9a shows the variation of stored thermal energy throughout the day on summer solstice with different TES hours with the SM of 2.2. The results indicate that the solar energy collected on summer solstice is in between 9-10 hours of TES capacity. Therefore, the stored thermal energy could be used to meet the energy demand requirement for at least 9 hours on summer solstice. Fig. 9b shows the variation of stored thermal energy throughout the day on winter solstice for different TES hours with the SM of 2.2. It is clearly shown that the characteristic curves for 6 to 10 hours hardly change, so the stored energy can only meet the energy demand requirement for 5 hours TES capacity. Fig. 9c shows the variation of stored thermal energy throughout the day on summer solstice with different SM when TES hour is 10. It can be seen from the figure

that, when $SM = 1.0$, the system can operate in the coupled mode for only 11 hours. While, the system can operate in the coupled mode for 23 hours when SM is 2.2. Fig. 9d shows the variation of stored thermal energy through the day on winter solstice with different SM when TES hour is 10 hours. It clearly shows that, for $SM = 1.0$ and 2.2, the STACP system can operate in coupled mode for 8 hours and 13 hours respectively.

5. Conclusions

In this study, the performance of the STACP system under 100% load, 75% load, and 50% load with different solar shares introduced are investigated and the maximum solar power that boiler can absorb under different loads are determined. Then, the effects of SM and TES hour on the daily performance of STACP system are investigated.

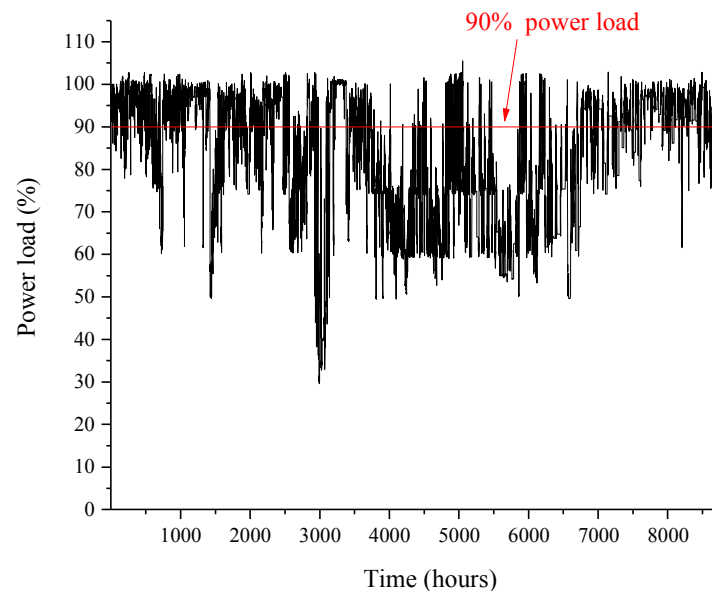
Results indicate that the maximum solar power that a 600 MW_e boiler can absorb at 100% load, 75% load and 50% load are 76.4 MW_{th} , 54.2 MW_{th} and 23.0 MW_{th} , respectively. In addition, the maximum saved standard coal consumption rates are 13.53 g/kWh , 12.81 g/kWh and 8.22 g/kWh , respectively. With the increase of solar power contribution, the boiler efficiency, system efficiency and solar thermal-to-power efficiency show a downward trend, while the power generation from the solar energy shows an upward trend. The studies of SM and thermal storage hour show that the daily coal consumption of summer solstice is lowest and the daily coal consumption of winter solstice is highest for a particular SM and thermal storage hour. Based on the design parameter of the solar field in this study, the study also found that, for all the four typical days, when the SM is 2.2, the solar energy collected per day still cannot meet the energy required for the boiler operating with $Q_{boiler,max}$ for 24 hours a day at 100% load and 75% load. While the solar energy collected per day can meet the energy required for the boiler operating with $Q_{boiler,max}$ input for 24 hours a day under

50% load, when SM is 1.8.

Acknowledgments

The research work is supported by National Major Fundamental Research Program of China (No. 2015CB251505), China National Natural Science Foundation (No. 51776063), the Fundamental Research Funds for the Central Universities (2016XS29, 2016YQ04), China Scholarship Council and Cranfield University.

Appendix A. Real-time power loads of a coal-fired power plant



References

- [1] Zhu Y, Zhai R, Qi J, Yang Y, Reyes-Belmonte MA, Romero M, et al. Annual performance of solar tower aided coal-fired power generation system. *Energy*. 2017;119:662-74.
- [2] Liu F, Lyu T, Pan L, Wang F. Influencing factors of public support for modern coal-fired power plant projects: An empirical study from China. *Energy Policy*. 2017;105:398-406.
- [3] Hofmann M, Tsatsaronis G. Comparative exergoeconomic assessment of coal-fired power plants – Binary Rankine cycle versus conventional steam cycle. *Energy*. 2018;142:168-79.
- [4] Li J, Wu Z, Zeng K, Flamant G, Ding A, Wang J. Safety and efficiency assessment of a solar-aided coal-fired power plant. *Energy Conversion and Management*. 2017;150:714-24.
- [5] Zhang M, Xu C, Du X, Amjad M, Wen D. Off-design performance of concentrated solar heat and coal double-source boiler power generation with thermochemical energy storage. *Applied Energy*. 2017;189:697-710.
- [6] Wu J, Hou H, Yang Y, Hu E. Annual performance of a solar aided coal-fired power generation system (SACPG) with various solar field areas and thermal energy storage capacity. *Applied Energy*.

2015;157:123-33.

[7] Zoschak RJ, Wu SF. Studies of the direct input of solar energy to a fossil-fueled central station steam power plant. *Solar Energy*. 1975;17(5):297-305.

[8] Hu E, Yang Y, Nishimura A, Yilmaz F, Kouzani A. Solar thermal aided power generation. *Applied Energy*. 2010;87(9):2881-5.

[9] Yang Y, Yan Q, Zhai R, Kouzani A, Hu E. An efficient way to use medium-or-low temperature solar heat for power generation – integration into conventional power plant. *Applied Thermal Engineering*. 2011;31(2-3):157-62.

[10] Hou H, Wu J, Yang Y, Hu E, Chen S. Performance of a solar aided power plant in fuel saving mode. *Applied Energy*. 2015;160:873-81.

[11] Li J, Yu X, Wang J, Huang S. Coupling performance analysis of a solar aided coal-fired power plant. *Applied Thermal Engineering*. 2016;106:613-24.

[12] Hong H, Peng S, Zhang H, Sun J, Jin H. Performance assessment of hybrid solar energy and coal-fired power plant based on feed-water preheating. *Energy*. 2017;128:830-8.

[13] Zhao Y, Hong H, Jin H, Li P. Thermodynamic mechanism for hybridization of moderate-temperature solar heat with conventional fossil-fired power plant. *Energy*. 2017;133:832-42.

[14] Wu J, Hou H, Yang Y. Annual economic performance of a solar-aided 600MW coal-fired power generation system under different tracking modes, aperture areas, and storage capacities. *Applied Thermal Engineering*. 2016;104:319-32.

[15] Adibhatla S, Kaushik SC. Energy, exergy, economic and environmental (4E) analyses of a conceptual solar aided coal fired 500 MWe thermal power plant with thermal energy storage option. *Sustainable Energy Technologies and Assessments*. 2017;21:89-99.

[16] Peng S, Hong H, Wang Y, Wang Z, Jin H. Off-design thermodynamic performances on typical days of a 330MW solar aided coal-fired power plant in China. *Applied Energy*. 2014;130:500-9.

[17] Zhao Y, Hong H, Jin H. Optimization of the solar field size for the solar–coal hybrid system. *Applied Energy*. 2017;185:1162-72.

[18] Zhong W, Chen X, Zhou Y, Wu Y, López C. Optimization of a solar aided coal-fired combined heat and power plant based on changeable integrate mode under different solar irradiance. *Solar Energy*. 2017;150:437-46.

[19] Sun J, Wang R, Hong H, Liu Q. An optimized tracking strategy for small-scale double-axis parabolic trough collector. *Applied Thermal Engineering*. 2017;112:1408-20.

[20] Zhai R, Li C, Chen Y, Yang Y, Patchigolla K, Oakey JE. Life cycle assessment of solar aided coal-fired power system with and without heat storage. *Energy Conversion and Management*. 2016;111:453-65.

[21] Peng S, Wang Z, Hong H, Xu D, Jin H. Exergy evaluation of a typical 330MW solar-hybrid coal-fired power plant in China. *Energy Conversion and Management*. 2014;85:848-55.

[22] Hou H, Xu Z, Yang Y. An evaluation method of solar contribution in a solar aided power generation (SAPG) system based on exergy analysis. *Applied Energy*. 2016;182:1-8.

[23] Wang R, Sun J, Hong H, Jin H. Comprehensive evaluation for different modes of solar-aided coal-fired power generation system under common framework regarding both coal-savability and efficiency-promotability. *Energy*. 2018;143:151-67.

[24] Zhang M, Du X, Pang L, Xu C, Yang L. Performance of double source boiler with coal-fired and solar power tower heat for supercritical power generating unit. *Energy*. 2016;104:64-75.

[25] Zhu Y, Zhai R, Peng H, Yang Y. Exergy destruction analysis of solar tower aided coal-fired power

- generation system using exergy and advanced exergetic methods. *Applied Thermal Engineering*. 2016;108:339-46.
- [26] Zhu Y, Zhai R, Yang Y, Reyes-Belmonte M. Techno-Economic Analysis of Solar Tower Aided Coal-Fired Power Generation System. *Energies*. 2017;10(12):1392.
- [27] Li C, Zhai R, Yang Y, Patchigolla K, Oakey JE. Thermal performance of different integration schemes for a solar tower aided coal-fired power system. *Energy Conversion and Management*. 2018;171:1237-45.
- [28] Xu C, Wang Z, Li X, Sun F. Energy and exergy analysis of solar power tower plants. *Applied Thermal Engineering*. 2011;31(17-18):3904-13.
- [29] Li C, Zhai R, Liu H, Yang Y, Wu H. Optimization of a heliostat field layout using hybrid PSO-GA algorithm. *Applied Thermal Engineering*. 2018;128:33-41.
- [30] Li C, Zhai R, Yang Y. Optimization of a Heliostat Field Layout on Annual Basis Using a Hybrid Algorithm Combining Particle Swarm Optimization Algorithm and Genetic Algorithm. *Energies*. 2017;10(12):1924.
- [31] Wagner MJ. Simulation and predictive performance modeling of utility-scale central receiver system power plants. Madison: University of Wisconsin, 2008.
- [32] Pacheco JE, Reilly HE, Kolb GJ, Tyner CE. Summary of the solar two test and evaluation program. Sandia National Labs., Albuquerque, NM (US); Sandia National Labs., Livermore, CA (US); 2000.
- [33] Lata JM, Rodríguez M, de Lara MÁ. High flux central receivers of molten salts for the new generation of commercial stand-alone solar power plants. *Journal of Solar Energy Engineering*. 2008;130(2):021002.
- [34] Jianfeng L, Jing D, Jianping Y. Heat transfer performance of an external receiver pipe under unilateral concentrated solar radiation. *Solar Energy*. 2010;84(11):1879-87.
- [35] Che D. Boilers: theory, design and operation: Xi'an Jiaotong University Press, 2008.